U(VI) sorption on Ca-bentonite at (hyper)alkaline conditions – Spectroscopic investigations of retention mechanisms

Philipp, T.; Shams Aldin Azzam, S.; Rossberg, A.; Huittinen, N.; Schmeide, K.; Stumpf, T.;

Originally published:

April 2019

Science of the Total Environment 676(2019), 469-481

DOI: https://doi.org/10.1016/j.scitotenv.2019.04.274

Perma-Link to Publication Repository of HZDR:

https://www.hzdr.de/publications/Publ-28474

U(VI) sorption on Ca-bentonite at (hyper)alkaline conditions – Spectroscopic investigations of retention mechanisms

Thimo Philipp[a], Salim Shams Aldin Azzam[a], André Rossberg[a,b], Nina Huittinen[a], Katja Schmeide[a,*], Thorsten Stumpf[a]

[a] Helmholtz-Zentrum Dresden - Rossendorf, Institute of Resource Ecology, Bautzner Landstraße 400, 01328 Dresden, Germany

[b] The Rossendorf Beamline at ESRF, F-38043 Grenoble, France

corresponding author:
Dr. Katja Schmeide
Helmholtz-Zentrum Dresden - Rossendorf, Institute of Resource Ecology
Bautzner Landstraße 400, 01328 Dresden, Germany
Telephone: +49 351 260 2436
Email: k.schmeide@hzdr.de

E-mail addresses: t.philipp@hzdr.de (T. Philipp), s.shams@hzdr.de (S. Shams), rossberg@esrf.fr (A. Rossberg), n.huittinen@hzdr.de (N. Huittinen), k.schmeide@hzdr.de (K. Schmeide), t.stumpf@hzdr.de (T. Stumpf).

Abstract

Environmental conditions in deep geological repositories for radioactive waste may involve high pH values due to the degradation of concrete. However, the U(VI) sorption at such (hyper)alkaline conditions is still poorly understood. In this study, batch sorption experiments with Ca-bentonite in the pH range 8-13 at different carbonate concentrations were combined with spectroscopic investigations in order to gain insight into the underlying retention mechanisms. It was found that U(VI) sorption strongly correlates with the aquatic U(VI) speciation determined by time-resolved laser-induced luminescence spectroscopy (TRLFS). Increasing retention with increasing pH was accompanied by a change in aquatic speciation from uranyl carbonates to uranyl hydroxides. The occurrence of luminescence line narrowing and a decreased frequency of the symmetric stretch vibration, deduced from site-selective TRLFS, indicate the presence of adsorbed U(VI) surface complexes. X-ray absorption fine structure (EXAFS) spectroscopy confirms that surface precipitation does not contribute to the removal of U(VI) from solution but that retention occurs through the formation of two non-equivalent U(VI)-complexes on the bentonite surface. The present study demonstrates that in alkaline environments, where often only precipitation processes are considered, adsorption can provide effective retention of U(VI), despite the anionic character of prevailing aqueous species.

Keywords: uranium, Ca-bentonite, site-selective TRLFS, EXAFS, speciation, surface complexation

1. Introduction

Radioactive waste originating from nuclear power plants, military, industrial and medical applications can pose a threat to human health due to its radio- and chemotoxic properties when migrating through the subsurface and entering the food chain. Among the radionuclides contained in the nuclear waste matrix, uranium is of special concern, since it represents by far the largest fraction of the waste and features high chemotoxicity and isotopes with an extremely long half-life (i.e. U-238, U-235). Therefore, a secure and effective disposal of such waste over long time spans within deep geological repositories has to be guaranteed. Long-term safety assessment regarding the mobility of uranium in the subsurface (safety case) requires profound understanding of uranium retention processes at mineral surfaces under near-field repository conditions. Such conditions can involve high ionic strengths and high pH values. Pore water chemistry of North German clay formations, which are considered as potential host rocks, is characterized by high ionic strengths with salinities of approx. 150 g/L in the lower cretaceous claystones at 800 m depth (Nowak and Maßmann, 2013; Wolfgramm et al., 2011). Groundwaters in Japanese clay rocks and Canadian limestones, also possible host rocks, feature similar ionic strengths (Hama et al., 2007; Mazurek, 2004). Such high salinities promote the degradation of concrete within the geo-engineered barrier of the repository, leading to the evolution of hyperalkaline cement pore waters ($10 < pH < 13$) (Berner, 1992; Gaucher et al., 2006; Seher and Bracke, 2012). Such a shift in pore water chemistry can radically alter the retention potential of mineral surfaces towards radionuclides. In this study the retention capability of Ca-bentonite is investigated, as this material is considered as buffer and backfill material within deep geological repositories (Lommerzheim and Jobmann, 2014).

While the sorption behavior of U(VI) by bentonite and its main constituent montmorillonite has been extensively studied at up to weakly alkaline conditions, its sorption affinity and the underlying mechanisms are largely unknown in the (hyper)alkaline regime. Under acidic conditions ($pH < 5$) and low ionic strengths, the uranyl (here always used for $U^{VI}O_2^{2+}$ only), present as fully solvated ion, binds via cation exchange on negatively charged surfaces with an overall low to moderate uptake. As the pH increases to the circumneutral range, various U(VI) hydrolysis complexes dominate the solution

speciation, which further can form inner-sphere sorption complexes at the montmorillonite edge sites (silanol and/or aluminol groups), resulting in a quantitative uptake of uranium by the clay mineral (Maher et al., 2013; Stumm, 1992). The U(VI) surface speciation investigated in EXAFS measurements confirmed a splitting of the equatorial oxygen shell of uranyl at circumneutral pH and backscattering contributions from substrate atoms (Si/Al, Fe), indicative of inner-sphere complexation. Shell fitting suggested bidentate coordination to aluminum octahedra and/or silicon tetrahedra (Catalano and Brown, 2005; Chisholm-Brause et al., 1994; Hennig et al., 2002; Marques Fernandes et al., 2012; Sylwester et al., 2000). In the presence of carbonate, sorption decreases drastically at pH > 7 due to the formation of negatively charged aqueous uranyl carbonate complexes. These complexes are extremely stable in solution (Guillaumont et al., 2003) and have a low tendency to attach to mineral surfaces (Fritsch, 2018; Maher et al., 2013; Marques Fernandes et al., 2012; Richter et al., 2016; Tournassat et al., 2018). Nevertheless, modelling by Marques Fernandes et al. (2012) suggested that uranyl carbonate complexes sorb at least to some extent to montmorillonite surfaces and also a number of spectroscopic studies indicate the formation of ternary uranyl carbonate surface complexes on montmorillonite, silica, Hanford sediment and ferrihydrite (Rossberg et al., 2009; Saleh et al., 2018; Troyer et al., 2016; Wang et al., 2005). On the other hand, Marques Fernandes et al. (2012) could not provide spectroscopic evidence for the formation of such surface complexes by EXAFS. Furthermore, Tournassat et al. (2018) were able to model U(VI) retention behavior under a wide range of chemical conditions without the introduction of uranyl carbonate surface complexes with the help of a refined surface complexation model based on the consideration of surface charge spillover effects and precise measurements of dissolved inorganic carbon (DIC). The presence of Ca^{2+} in the solution can further modify the U(VI) retention behavior. Formation of highly soluble ternary $CaUO_2(CO_3)_3^{2-}$ and $Ca_2UO_2(CO_3)_{3\,(aq)}$ complexes can additionally suppress U(VI) adsorption (Bernhard et al., 2001; Joseph et al., 2013; Meleshyn et al., 2009; Schmeide et al., 2014).

None of the studies dealing with the formation of uranyl carbonate complexes address if such complexes still prevail when further increasing the pH value. No clear upper pH boundary for their formation has been shown experimentally as a function of DIC due to increasing competition of carbonate with the hydroxyl ligand. Beside uranyl carbonates, the aqueous speciation in the pH range

8-13 is dominated by the higher hydrolysis complexes of uranyl ($UO_2(OH)_3^-$ and $UO_2(OH)_4^{2-}$) (Figure SM1). Generally, almost no studies were published on the adsorption of U(VI) by clay at pH > 10, describing surface complexes formed by contribution of these anionic aqueous U(VI) species. In his thesis, A. Schnurr (2015) quantified the U(VI) retention by illite and kaolinite up to pH 12. For both minerals almost complete sorption was maintained up to pH 11. At pH above that, a slight decrease in sorption was observed. Possible explanations for the observed retention behavior were not pursued spectroscopically. The mentioned study was performed in the absence of CO_2. To our knowledge, no U(VI) sorption study on clay minerals at (hyper)alkaline pH exists, which would additionally consider the effect of carbonate in the solution at pH 10-13. Studies concerning the U(VI) retention at hyperalkaline conditions mainly address colloid formation or precipitation processes. Generally, U(VI) solubility in (hyper)alkaline solutions is very low and (earth) alkali uranates are the solubility limiting phases (Altmaier et al., 2017; Bots et al., 2014; Tits and Wieland, 2018; Yamamura et al., 1998). In carbonate-free NaCl solutions at pH 8-11, Altmaier et al. (2017) determined the U(VI) solubility, controlled by $Na_2U_2O_7 \cdot H_2O$(cr), to be at nanomolar concentrations (I=2.6 M). In Ca-containing solutions, U(VI) preferentially precipitates as Ca-uranate ($CaUO_4$(s)) (Ochs et al., 2016; Tits et al., 2011; Tits and Wieland, 2018). Above pH 11, U(VI) solubility increases, reaching micromolar concentrations at pH 13 (Altmaier et al., 2017). Kaplan et al. (1998) investigated the U(VI) retention by sediments up to pH 12 and observed a number of heterogeneous precipitation processes. Kenney et al. (2017) attributed the removal of U(VI) from the solution above pH 10 to the precipitation of uranyl carbonates. Smith et al. (2015) observed the formation of U(VI) colloids and surface mediated precipitation processes in hyperalkaline calcite systems in most of their experiments. Indications for the formation of U(VI) surface complexes on calcite at pH 10.5 and 13.3 were only observed at sub-micromolar U(VI) concentrations. Also Bots et al. (2014) observed the formation of U(VI) nanoparticles at pH > 13. Considerable research has been performed concerning the U(VI) immobilization in cementitious systems at pH > 13. U(VI) is effectively retained in calcium silicate hydrate (C-S-H) phases and hardened cement paste (HCP) (Ochs et al., 2016; Tits et al., 2008; Wieland, 2014; Wolter et al., 2019) and uptake is facilitated by the presence of dissolved calcium (Pointeau et al., 2004; Tits and Wieland, 2018). Spectroscopic studies further investigated the nature

of the retained U(VI) complexes. TRLFS revealed the presence of surface complexes as well as incorporated species and precipitation of Ca-uranates (Tits et al., 2011; Tits et al., 2015). EXAFS investigations suggested a local coordination environment similar to U(VI) silicates (such as uranophane) with a split equatorial oxygen shell and short and long silicon distances (Harfouche et al., 2006; Macé et al., 2013). Despite all the above mentioned findings, U(VI) sorption in (hyper)alkaline systems is still poorly understood as the existing studies provide only insight at very specific solution conditions (pH, carbonate concentration, etc.), with even sometimes contradictory results, mostly lacking information on the molecular level.

Due to the scarcity of thermodynamic data, so far no reliable model prediction can be made regarding both the aquatic and the surface speciation of U(VI) under (hyper)alkaline conditions. Therefore, the present work aims to provide a comprehensive and systematic description of the U(VI) sorption behavior on Ca-bentonite in the pH range 8-13 as a function of pH and carbonate concentration. In addition, laser luminescence spectroscopy and X-ray absorption spectroscopy applied in the present study deliver information about the underlying retention mechanisms (i.e. distinguish between surface complexation and surface precipitation) and the local U(VI) coordination environment of the retained species.

2. Material and Methods

2.1. Material

The Ca-bentonite used as sorptive was of the type *Calcigel*® (Clariant, München, Germany). This naturally occurring clay rock is mined in Bavaria (Germany) and was received as a powder with particle sizes between 0.5 and 150 µm, the dominant fraction (90 %) of the particles being smaller than 90 µm (laser granulometer HELOS Series KF + Quixel (SYMPATEC, Clausthal-Zellerfeld, Germany), range "R3": 0.5-75 µm). The BET specific surface area was determined to be 76.5 ± 0.3 m^2/g (Beckman Coulter, Fullerton, USA). The mineral composition according to the supplier is 60-70 % montmorillonite, 6-9 % quartz, 1-6 % mica, 1-4 % feldspar, 1-2 % kaolinite and 5-10 % others.

As background electrolyte a mixed salt solution (referred to as 'diluted Gipshut solution') was used in all experiments, consisting of 2.5 M NaCl (p.a., Carl Roth, Karlsruhe, Germany), 0.02 M $CaCl_2$ (puriss. AppliChem, Darmstadt, Germany), 0.02 M Na_2SO_4 (p.a., Merck, Darmstadt, Germany) and 0.0051 M KCl (p.a., Merck). Featuring a total ionic strength of 2.63 M, it simulates in situ pore waters of North German clay and salt formations at hypothetical repository depth (Wolfgramm et al., 2011). All solutions were prepared with deionized water (18 MΩ cm^{-1}; mod. Milli-RO/Milli-Q-System, Millipore, Schwalbach, Germany). For all experiments under N_2 atmosphere, water was additionally degassed prior to solution preparation. U(VI) addition was realized with a 1×10^{-3} M stock solution (U_{nat} in 0.005 M $HClO_4$). Carbonate was introduced to the samples by adding aliquots of 1 M $NaHCO_3$ (p.a., Carl Roth) or 2 M Na_2CO_3 (p.a., Merck) stock solutions.

2.2. Bentonite characterization at (hyper)alkaline conditions

In order to evaluate the stability of Ca-bentonite towards treatment with alkaline solutions, leaching tests were performed as a function of pH. Duplicate samples of 10 g/L Ca-bentonite were contacted with 0.1 M NaCl solution for three weeks at pH 8-13 (increments of 0.5). Frequent pH adjustments (every two or three days) were done with NaOH (p.a., Carl Roth) and HCl (p.a., ACS, ISO, Carl

Roth). After centrifugation (6800×*g*, 30 min) in an Avanti J-20 XP centrifuge (Beckman Coulter, Fullerton, USA), the supernatant was analyzed for Na, Mg, Al, Si, K and Ca with ICP-MS (NexION 350X, PerkinElmer, Waltham, USA), and for CO_3^{2-} with total inorganic carbon measurements (multiN/C 2100, Analytik Jena, Germany). The centrifugate was analyzed with the powder X-ray diffractometer Rigaku MiniFlex 600 (Tokyo, Japan), using Cu Kα radiation and a Bragg-Brentano geometry (in θ-2θ geometry) with a step size of 0.02 °2θ and a speed of 0.92 steps per second. For mineral phase identification, the ICDD PDF database was used.

The surface charge of Ca-bentonite particles was determined by zeta potential measurements (Zetasizer Nano ZS, Malvern Instruments, Malvern, United Kingdom). 11 bentonite suspensions (0.1 g/L) in the pH range 8-13 were prepared in 0.1 M NaCl, 2.5 M NaCl and 0.1 M NaCl + 0.02 M $CaCl_2$ in order to evaluate the effect of pH, ionic strength and calcium concentration. Potentials were averaged over ten measurements consisting of 10-50 scans.

2.3. Batch sorption experiments

All samples were prepared in duplicate. Bentonite powder was weighed in polypropylene centrifuge tubes and was suspended with 10 mL diluted Gipshut solution. As a result of experiments with variable bentonite mass (Figure SM2), a solid to liquid (S/L) ratio of 10 g/L was selected for all sorption experiments. Suspensions were pre-conditioned with frequent pH-adjustments with diluted NaOH or HCl (every two or three days) until a constant pH value (±0.05) was reached (approx. two weeks). The pH was measured with an InoLab pH 7110 pH meter (WTW, Weilheim, Germany) and a SenTix MIC glass electrode (WTW). Three point calibration of the pH meter was executed with WTW buffer solutions (pH 6.865, 9.180 and 12.454) (WTW).

In solutions with high ionic strengths, the measured potential at the pH electrode, and accordingly the derived pH_{exp}, deviates from the true potential due to the great discrepancy between the activity coefficients of the sample and the electrolyte of the electrode (Altmaier et al., 2003). By introducing a correction parameter A, the true pH can be derived according to:

$$-\log[H^+] = pH_{exp} + A \quad (1)$$

A was determined to be ~0.4 for this system by measuring the pH of solutions with an ionic strength of 2.63 M and known H^+ or OH^- concentrations. During pre-equilibration, samples were placed in an end-over-end shaker.

After pre-equilibration, U(VI) was added to the suspensions by pipetting calculated volumes of the U(VI) stock solution. The initial U(VI) concentrations of each experiment are summarized in Table 1. The sorption time was always seven days during which the samples were rotated in an end-over-end shaker. This reaction time was based on kinetic sorption experiments (Figure SM3).

For phase separation, samples were centrifuged at 6800×g for 30 min (see above). Photon correlation spectroscopy (Zetasizer Nano ZS) showed that this procedure led to a sufficient phase separation, leaving no measurable particle fraction in solution.

Uranium concentrations in the supernatants were determined by ICP-MS (see above). From the initial (c_0) and the equilibrium (c_{eq}) U(VI) concentrations in solution [M], the sorption distribution coefficient K_d was calculated according to equation (2), where V [L] is the volume of the solution and m [kg] the mass of the solid.

$$K_d = \frac{c_0 - c_{eq}}{c_{eq}} \times \frac{V}{m} \quad (2)$$

Experiments were carried out both at carbonate-free conditions (N_2 inert gas box) and in the presence of carbonate (at ambient air conditions). Low dissolved carbonate (LC = 1 mM) and high carbonate (HC = 100 mM) concentrations were achieved by adding calculated amounts of $NaHCO_3$ or Na_2CO_3 to the solutions. These concentrations are representative of the lower and upper boundary for natural carbonate concentrations expected in pore waters in the North German Basin at repository depth (approx. 800 m). Analytical determination of the carbonate content (see above) confirmed stable concentrations of dissolved carbonate within the time frame of the experiments. CO_2 from the ambient air did not lead to an additional measureable increase of carbonate concentration within the time frame of the experiments.

Samples without Ca-bentonite were prepared in order to investigate the solubility of U(VI) in the bentonite leachate under the given experimental conditions. As polypropylene centrifuge tubes showed significant uptake of U(VI) in the absence of Ca-bentonite (Text SM1), for these experiments fluorinated ethylene propylene (FEP) vials (Thermo Scientific Nalgene, Waltham, USA) were used, featuring an inert surface that minimizes uranium adsorption. Leachates of Ca-bentonite were produced at different pH values by contacting it with diluted Gipshut solution (10 g/L) for 2 weeks with continuous pH adjustments (pH 8-12.5, increments of 0.5). After phase separation, U(VI) was added to 10 mL of the leachate to reach a U(VI) concentration of 5×10^{-7} M. Seven days after U(VI) addition, the samples were ultracentrifuged (60 min, 187000×*g*, Optima XL 100K, Beckman Coulter) and the supernatants were analyzed for uranium with ICP-MS.

In Table 1 all performed batch experiments and relevant experimental conditions are summarized.

Table 1: Overview of performed batch experiments. Diluted Gipshut solution (I=2.63 M) was used as background electrolyte in all experiments. 'N_2' refers to experiments in the absence of CO_2 (minimal carbonate concentrations originating from bentonite leaching), 'LC' to low carbonate concentrations (1 mM) and 'HC' to high carbonate concentrations (100 mM).

Experiment	S/L ratio [g/L]	atmosphere	c(U) [M]	pH
Solubility	-	N_2	5×10^{-7}	8-13
Leaching	1-20	N_2 LC	-	8-13
S/L ratio dependency	3-20	N_2 LC	1×10^{-6}	8
Kinetics	10	N_2 LC	1×10^{-6}	8
pH dependency	10	N_2 LC HC	5×10^{-7} 1×10^{-6} 1×10^{-6}	8-13

2.4. Time-resolved laser-induced luminescence spectroscopy (TRLFS)

In U(VI) luminescence spectroscopy, laser light is used to excite an electron from the covalently bound oxygen atoms of the "yl"-cation via a charge transfer mechanism to unoccupied molecular orbitals of uranium. The relaxation from the excited state to the electronic ground state will give rise to emission of photos (luminescence). The released energy of photons corresponds to the transition to the lowest vibrational level of the degenerated ground state (electronic transition line E) and to the higher vibronic levels of the electronic ground state (lines of vibronic progression S_1, S_2, etc.), yielding the characteristic multi-peak spectrum of uranyl. The spacing between E_1 and S_1, defined as ν_s, represents the total symmetric stretch vibration frequency of the uranyl moiety (Tits et al., 2015; Wang et al., 2005). The magnitude of this frequency is sensitive to the number and type of ligands present in the equatorial plane and can be taken as a measure of the binding strength of coordinating ligands. An increased binding strength of equatorially bound ligands will withdraw electron density from the axial oxygens, reducing the strength of the "yl"-bond which in turn reduces the total symmetric stretch vibration frequency. Thus, a smaller E_1 to S_1 spacing is indicative of stronger bonding.

Conventionally, U(VI) luminescence is measured after indirect excitation with a high incident laser energy so that all U(VI) species contained in the sample are excited simultaneously. In case of a large heterogeneity of bonding environments (species or sorption sites) within the sample, this will lead to broadened and poorly resolved spectra. This broadening can be overcome by applying site-selective TRLFS at liquid helium temperatures. With this technique single species within the sample can be excited selectively by varying the excitation energy. At each wavelength within the inhomogeneously broadened absorption band only a small subset of uranyl ions is excited directly to the lowest vibrational level of the excited state, decaying radiatively to the ground state. For a more detailed explanation we refer to Tits et al. (2015), who applied this technique successfully for the first time for U(VI).

The aqueous speciation of uranium in the diluted Gipshut solution was investigated with non-selective TRLFS at λ_{ex} = 266 nm. Measurements were performed in the absence of CO_2, at low and at high carbonate concentrations, equivalent to the pH-dependent sorption studies. Batch samples with

uranium concentrations of 5×10^{-7} M in diluted Gipshut solution were prepared in FEP vials at pH 8-13. After 7 days, with frequent pH adjustments, 1 mL of each sample was filled in a polystyrene one time cuvette (Carl Roth) and quick-freezed with liquid nitrogen. TRLFS measurements were performed at 153 K by using a cryogenic cooling system. The laser system used was a Nd:YAG laser (Minilite high-energy solid-state laser; Continuum, San Jose, USA) as described in Steudtner et al. (2011) operating at an average pulsed energy of 0.3 mJ. The emission of the samples was recorded using an iHR550 spectrograph (HORIBA Jobin Yvon, Bensheim, Germany) and an ICCD camera (HORIBA Jobin Yvon). A gate width of 2000 µs and a slit width to the spectrograph of 2000 µm were chosen. Spectra were recorded at different delay times (t_i), defined by the equation $t_i = 0.1 + 0.005 \cdot x + i^{4/2000}$, with *i* being the step number. At each time step, 100 measurements were averaged. Peak positions were identified from second derivatives of FFT-filter smoothed spectra by determining their negative maxima. Luminescence lifetimes were obtained by plotting cumulative intensities at each time step against delay time. Data points were then fitted exponentially.

Site-selective TRLFS was applied to investigate the U(VI) species sorbed on the Ca-bentonite surface. Samples were prepared as described above in the batch sorption experiments, but with lower S/L ratio (0.3 g/L) in order to increase the U(VI) surface coverage. Two samples were prepared in the absence of CO_2 at pH 11, where sorption is at maximum: One with the same U(VI) concentration as in the pH-dependent sorption experiments (5×10^{-7} M) and one with a U(VI) concentration two orders of magnitude higher than that (5×10^{-5} M) to provoke U(VI) precipitation for comparison. After ultracentrifugation (187000×*g*) (see above) each wet paste pellet was transferred into a copper sample holder with a sealable quartz glass lid. Measurements were performed with a pulsed Nd:YAG (Continuum Surelite II, San Jose, USA) pumped dye laser setup (Radiant Dyes Narrow Scan K, Wermelskirchen, Germany). The emitted luminescence emission light was directed into a spectrograph (Shamrock 303i, Andor Oxford Instruments, Abingdon, United Kingdom) equipped with a polychromator with 300, 600, and 1200 lines/mm gratings, and the emission was monitored with an intensified CCD camera (Andor iStar, Oxford Instruments) 10 µs after the exciting laser pulse in a time window of 10 ms. The laser pulse energy and the exact excitation wavelength were monitored in every measurement with an optical power meter (Newport 1918-R, Irvine, USA) and a wavelength

meter (High Finesse WS-5, Tübingen, Germany), respectively. Spectra were recorded at excitation wavelengths between 460 and 520 nm with a step size of 0.2 nm. Additionally, time-resolved luminescence spectra were recorded at selected excitation wavelengths with a temporal step size of 10 µs. To achieve the desired spectral resolution the solid samples were cooled to ~10 K in a helium-refrigerated cryostat.

2.5. Extended X-ray absorption fine structure (EXAFS) spectroscopy

Batch sorption samples for the EXAFS measurements were prepared as described above. A total of 10 samples (Table SM1) with variable pH and carbonate concentration was prepared with a S/L ratio of 0.3 g/L, leading to sufficiently high surface coverage, despite the low initial U(VI) concentrations of 5×10^{-7} M in the absence of CO_2 and 1×10^{-6} M at low and high carbonate concentrations. Phase separation was achieved by ultracentrifugation, after which the Ca-bentonite wet paste was transferred into polyethylene (PE) sample holders. Samples were covered with capton tape, enclosed with a PE cap and finally sealed by soldering.

The U L_{III}-edge (17166 eV) EXAFS spectra were recorded at the Rossendorf Beamline (ROBL, BM20) at the European Synchrotron Radiation Facility (ESRF) (Matz et al., 1999), operated at 6 GeV and an electron current of 200 mA. For rejection of higher harmonics two Rh-coated mirrors were used and the incident white X-rays were monochromatized with a liquid nitrogen cooled Si(111) double crystal monochromator. The sorption samples were measured under cryogenic conditions (15 K) by using a closed cycle He-cryostat. In order to increase the signal-to-noise ratio for each sorption sample, a maximum of eleven fluorescence spectra were recorded by counting the signal of the U $L\alpha_{1,2}$ fluorescence lines with a 13-element Ge-detector. For energy calibration the absorption of a Y metal foil at the K-edge (17038 eV) was measured simultaneously during each energy scan. The incident photon flux and the absorption were measured with gas filled ionization chambers. For the calculation of the photoelectron wave vector (k) the ionization potential (E_0) was set arbitrarily to E_0 = 17185 eV. EXAFSPAK (George and Pickering, 1995) and WinXAS (Ressler, 1998) were used for the data treatment which included a correction for the dead-time of the 13 fluorescence channels, energy

calibration, averaging of the multiple sample scans, isolation of the EXAFS signal from the averaged data and shell fit. As a reference for the aqueous $UO_2(OH)_4^{2-}$ complex we used published data from (Moll et al., 2014), where six absorption spectra were measured at room temperature. For the shell fit theoretical scattering phase and amplitude functions were calculated with the ab-initio scattering code FEFF 8.20 (Ankudinov et al., 1998) by using an arbitrary structural model of the sorption complex and of the aqueous $UO_2(OH)_4^{2-}$ complex (Figure SM4).

Iterative target transformation factor analysis (ITFA) (Rossberg et al., 2003) was applied in order to quantify the structurally different sorption complexes and to isolate their spectra from the EXAFS spectral mixtures of the sorption samples (Text SM2).

3. Results and Discussion

3.1. Bentonite stability and surface charge

Leaching experiments and consecutive powder X-ray diffraction (PXRD) measurements prove a general stability of the minerals within the Ca-bentonite up to pH 12.5 over a time span of three weeks, so that the U(VI) sorption processes can be discussed without consideration of substantial disaggregation or alteration of the mineral surfaces. Ions leached from the Ca-bentonite to noticeable amounts are Ca, Mg, Si and Al (Figure SM5). The most strongly leached element up to pH 12 is calcium (~1.3 mM), which, however, is removed from the solution by calcite precipitation (in the presence of carbonate, not shown) above pH 8.5 and by portlandite ($Ca(OH)_2$) precipitation (in the absence of carbonate) above pH 12. Magnesium precipitates as brucite ($Mg(OH)_2$) above pH 9. Al and Si concentrations in the leachates are very low up to pH 12.5. Only at pH 13 a significant increase in concentration of both elements due to dissolution of montmorillonite can be observed. PXRD diffractograms of Ca-bentonite leached between pH 8.5 and 12.5 have a very similar appearance and feature the same main peaks (Figure SM6). Major identified phases are quartz and the clay minerals montmorillonite, illite and muscovite. No significant alteration of mineral composition with increasing pH could be detected. The observed stability of bentonite up to pH 12.5 is in accordance with literature. Several studies describe that treatment with alkaline fluids of pH 12.5 only lead to minimal alteration of smectites or leave the bentonite virtually unchanged (Fernández et al., 2009; Milodowski et al., 2016; Vuorinen et al., 2006). Additionally, Schatz et al. (2013) found that Ca-montmorillonite is more stable towards chemical erosion than Na-montmorillonite. Severe alterations only occur at even higher pH values (>13), higher temperatures and over longer timespans.

Zeta potential measurements show a negative surface charge of the Ca-bentonite over the entire pH range in 0.1 M NaCl (Figure SM7), as it can be expected from the permanent negative charge of 2:1 clay minerals due to isomorphous substitution of cations within the octahedral and tetrahedral layers. At high ionic strength (2.5 M NaCl) the potential is generally less negative because of the high density

of cations close to the surface. The addition of much smaller amounts of calcium (0.02 M) to 0.1 M NaCl results in a similar effect, indicating the adsorption of calcium to the clay mineral surface.

3.2. Batch sorption experiments

Batch sorption experiments exhibit a complex U(VI) retention behavior depending on pH and the amount of carbonate present in solution (Figure 1). In the absence of CO_2, U(VI) retention is approx. 90 % at pH 8-9 (squares in Figure 1). At higher pH, sorption even increases, forming a plateau of complete retention from pH 9.5 to about pH 12. At pH $\geq$ 12, U(VI) sorption decreases again to only 50 % at pH 13. At low carbonate concentration (1 mM), U(VI) retention is low (approx. 20 %) at pH 8-9. Going to higher pH values, the retention increases drastically, following a similar pH-dependent trend as in the absence of CO_2. Also here a plateau of complete sorption is observed at pH 10-12, followed by a pronounced drop at pH $\geq$ 12 (triangles in Figure 1). When carbonate concentration is high (100 mM), U(VI) retention remains on a very low level (< 10 %) up to pH 11. Thereafter it increases, reaching 80 % at pH 12 (diamonds in Figure 1), before dropping again, similar to the previously described series. The complete U(VI) retention in the absence of CO_2 and at low carbonate concentrations corresponds to maximum log(K_d) values of approx. 5-6 log(L/kg), restricted by the detection limit of the ICP-MS measurements (0.1 µg/L). At high carbonate concentrations, the maximum retention at pH 12 corresponds to a log(K_d) value of 2.6 log(L/kg) (Figure SM8). The lower U(VI) retention in the presence of carbonate at pH 8 to 9.5 is in accordance with literature and is attributed to the predominant formation of weakly sorbing (calcium) uranyl carbonate complexes (Bachmaf et al., 2008; Joseph et al., 2013; Maher et al., 2013; Marques Fernandes et al., 2012; Richter et al., 2016; Tournassat et al., 2018). The higher the carbonate concentration is, the stronger the U(VI) sorption decreases, as the relative abundance of uranyl carbonate species compared to uranyl hydroxides or mixed uranyl carbonate hydroxo complexes is higher. An increase in retention with further increasing pH has not been reported for such systems as none of these studies expands to the hyperalkaline regime. Also in the absence of CO_2 published data is scarce (see section 1). Even without discussing the underlying retention mechanism on a molecular level, the presented batch results alone provide already substantial knowledge gain as they present for the first time a systematic

study of the U(VI) retention by clay rock from weakly alkaline to hyperalkaline pH. The results show that sorption can be very effective up to pH 12, also in the presence of carbonate. The decreased U(VI) retention in the presence of carbonate, reported previously in the literature, does only apply up to a certain pH and is highly dependent on the amount of carbonate in the solution.

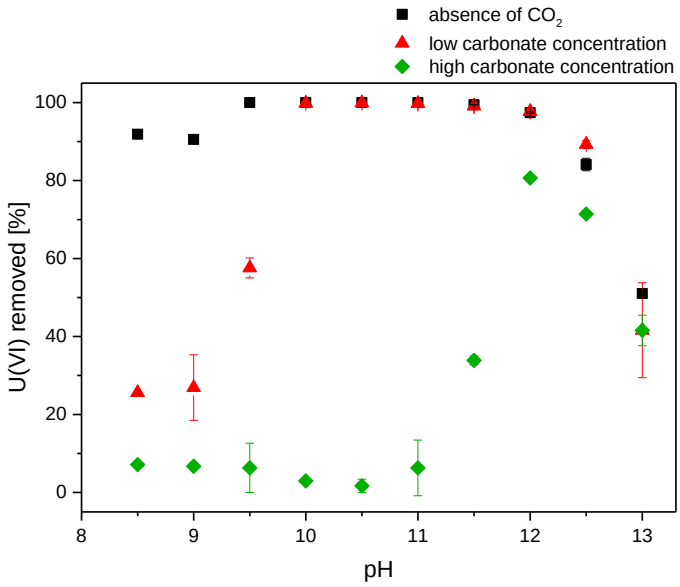

Figure 1: Percentage of U(VI) sorbed on Ca-bentonite (10 g/L) in dil. Gipshut solution (I = 2.63 M) as function of pH and carbonate concentration (see section 2.3). Initial U(VI) concentrations were 1×10^{-6} M in the presence and 5×10^{-7} M in the absence of carbonate.

3.3. Aqueous U(VI) speciation studied with TRLFS

In the absence of CO_2, the luminescence spectra of U(VI) in diluted Gipshut solution measured at 153 K feature a low intensity with a poor spectral resolution (Figure 2a). Both phenomena are characteristic for uranyl hydroxide complexes at alkaline conditions. This has been reported by Drobot et al. (2016); Martínez-Torrents et al. (2013), and Moulin et al. (1998), where monomeric hydrolysis species $UO_2(OH)_2$, $UO_2(OH)_3^-$ and $UO_2(OH)_4^{2-}$ were shown to exhibit broadened spectra with weak spectral splitting. In spite of the low signal to noise ratio (particularly up to pH 10), the positions of the first two main peaks could be identified, situated at approx. 500 nm and 521 nm for the samples up to pH 12 (Table 2). Drobot et al. (2016) observed maxima at 499 and 520 nm for $UO_2(OH)_{2\,(aq)}$ and at 503 and 525 nm for $UO_2(OH)_3^-$. Martínez-Torrents et al. (2013) and Moulin et al. (1998) described peaks for $UO_2(OH)_3^-$ at 503 and 521 nm and at 499 nm and 519 nm, respectively. Luminescence

lifetimes depend on the presence of quenchers and, to a large degree, on the temperature of the sample. Therefore, comparing lifetimes obtained in different studies is difficult. From the aforementioned studies only Martínez-Torrents et al. (2013) performed measurements at cryogenic conditions (10 K). The reported luminescence lifetime of 198 µs for $UO_2(OH)_3^-$ fits very well to the 208 µs obtained in the present work at pH 11 (measured at 153 K). At pH 13 the luminescence spectrum is shifted towards lower wavelength, having the first two maxima at approx. 490 and 511 nm (Table 2). These positions are in agreement with spectra measured by Tits et al. (2011) at very alkaline conditions (pH 13.3), which were assigned to the higher hydrolysis species $UO_2(OH)_4^{2-}$. The luminescence lifetime at pH 13 was measured to be somewhat shorter than at lower pH. This observation is consistent with the works of Martínez-Torrents et al. (2013) and Kitamura et al. (1998) in which shorter lifetimes are reported for $UO_2(OH)_4^{2-}$ compared to $UO_2(OH)_3^-$. Consequently, based on analysis of peak positions and luminescence lifetimes, anionic uranyl hydroxides (first $UO_2(OH)_3^-$ and at very high pH $UO_2(OH)_4^{2-}$) dominate the aqueous speciation of U(VI) in the diluted Gipshut solution in the absence of CO_2 between pH 8 and 13.

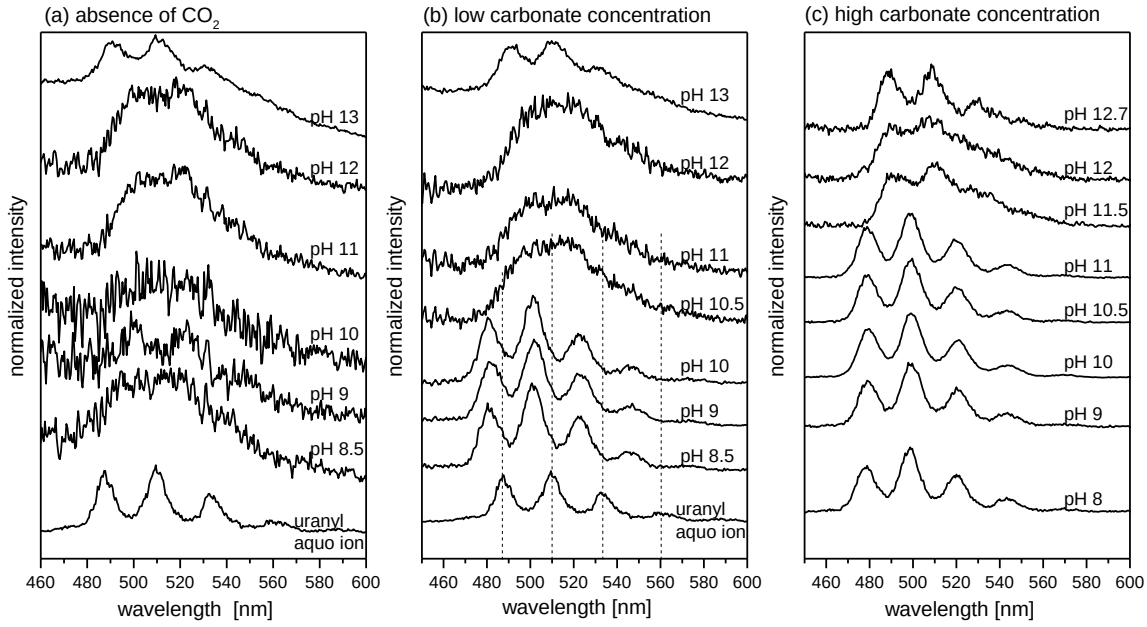

Figure 2: Luminescence spectra of uranyl ([U(VI)] = 5×10^{-7} M) in the diluted Gipshut solution as a function of pH in the absence of CO_2 (a), at low carbonate concentration (b) and at high carbonate concentration (c).

In the presence of carbonate, the recorded luminescence emission spectra vary strongly within the investigated pH range 8-13. Up to pH 10 at low carbonate concentration and up to pH 11 at high

carbonate concentration, the shape of the spectra is very similar, exhibiting a well-resolved spectral splitting (Figure 2b,c). Compared to the uranyl aquo ion, these spectra are shifted towards lower wavelengths, which is characteristic for uranyl carbonate complexes (Bernhard et al., 2001; Lee and Yun, 2013; Steudtner et al., 2011; Wang et al., 2004). The obtained peak positions match very well with literature data for $UO_2(CO_3)_3^{4-}$ and the ternary calcium uranyl carbonate complexes $Ca_2UO_2(CO_3)_{3\ (aq)}$ and $CaUO_2(CO_3)_3^{2-}$ (Table 2). Luminescence lifetimes of these samples range between 800 and 900 µs. As peak positions are very similar and the luminescence lifetimes depend on temperature and solution composition, it is not possible to distinguish between $UO_2(CO_3)_3^{4-}$ and ternary Ca-UO_2-CO_3 complexes here, based on the spectral properties. However, given that the diluted Gipshut solution contains large amounts of calcium, the formation of ternary complexes with calcium is expected. Another plausible complex is $MgUO_2(CO_3)_3^{2-}$, which was described by Lee et al. (2017) with almost the same luminescence spectroscopic properties as $UO_2(CO_3)_3^{4-}$. The formation of this complex might be favored when calcium is removed successively from the solution with increasing pH due to calcite precipitation. Magnesium is then still available as brucite precipitation is initiated at somewhat higher pH. At pH 10.5 at low carbonate concentrations and at pH 11.5 at high carbonate concentration, an abrupt change in speciation is visible. The well resolved emission bands are not detectable anymore. Instead, broad spectra with lower luminescence intensity are observed. Peak positions and lifetimes compare very well to those that were obtained in the absence of CO_2 (for a comparison, see Figure SM9) and are therefore also interpreted as monomeric uranyl hydroxide complexes $UO_2(OH)_3^-$ and $UO_2(OH)_4^{2-}$. Consequently, uranyl carbonate complexes, which have been widely reported to dominate the aqueous U(VI) speciation at alkaline conditions, prevail only up to a certain pH, depending on the concentration of dissolved carbonate. At higher pH, the formation of uranyl hydroxides is favored.

A clear correlation between changes in aqueous speciation and changes in the sorption behavior can be observed. U(VI) retention is low in the pH range, where uranyl carbonate complexes dominate the aqueous speciation according to the TRLFS measurements. The observed increase in retention in the presence of carbonate above a certain pH coincides with the change in aqueous speciation from uranyl carbonates to uranyl hydroxides. Generally, it can be stated that U(VI) retention is very high in

samples, where $UO_2(OH)_3^-$ dominates the aqueous speciation. At pH > 12 the decrease in retention correlates with the formation of the higher hydrolysis species $UO_2(OH)_4^{2-}$. In the light of electrostatic interactions, it has to be discussed if the very strong U(VI) retention at pH 10-12 can be attributed to adsorption of a negatively charged metal complex to the negatively charged bentonite surface, or if the retention under these conditions is rather caused by a precipitation of uranates.

Table 2: Luminescence spectroscopic properties (band positions and luminescence lifetimes) of U(VI) in the diluted Gipshut solution of selected samples at different pH and carbonate concentrations. Literature data are given for comparison.

Series	pH	Peak positions [nm]				Lifetime [µs]	T [K]
N_2	9.0	502.1	522.9			-	153
	11.0	499.3	521.0			208 ± 30	153
	13.0	490.4	510.7	531.6		74 ± 17	153
LC	9.0	481.2	502.1	523.4	546.9	877 ± 17	153
	11.0	497.0	519.2	542.8	569.6	149 ± 13	153
	13.0	490.4	510.3	532.5		89 ± 7	153
HC	9.0	478.8	499.6	521.4	544.1	804 ± 17	153
	11.0	477.9	499.2	520.5	544.1	808 ± 18	153
	12.7	488.1	508.9	530.2		112 ± 10	153
$UO_2(CO_3)_3^{4-}$ [a]		480.7	499.9	520.3	542.5	834 ± 9	153
$Ca_2UO_2(CO_3)_{3\,(aq)}$ [b]		480.5	501.2	522.7	546.0	1282	6
$UO_2(OH)_3^-$ [c]		503.0	521.0	534.0	550.0	198 ± 8	10
$UO_2(OH)_3^-$ [d]		503	525	547	572	3.4 ± 0	274
$UO_2(OH)_4^{2-}$ [e]		491.4	510.5			140 ± 30	153

[a] Steudtner et al. (2011); [b] Wang et al. (2004); [c] Martínez-Torrents et al. (2013); [d] Drobot et al. (2016); [e] Tits et al. (2011)

3.4. U(VI) solubility

Batch samples of U(VI) in leachates of Ca-bentonite in diluted Gipshut solution demonstrate that substantial amounts of the initial U(VI) (5×10^{-7} M) remained in solution over the entire pH range after

446 one week of contact time and after ultracentrifugation (Figure SM10). Hence, the complete removal of
447 U(VI) observed for the sorption samples at pH 10-12 cannot exclusively be attributed to precipitation
448 from the solution. This is in contrast to literature solubility studies, where U(VI) solubility is often
449 described to trend to nanomolar concentrations at alkaline conditions (Altmaier et al., 2017; Kitamura
450 et al., 1998). The solubility limiting phase between pH 8 and 13 is sodium di-uranate ($Na_2U_2O_7 \cdot H_2O$)
451 in pure sodium chloride solutions (Altmaier et al., 2017) and calcium uranate ($CaUO_4$) in the presence
452 of calcium (Bots et al., 2014; Moroni and Glasser, 1995; Smith et al., 2015; Tits et al., 2008; Tits et
453 al., 2011; Tits and Wieland, 2018). Due to the high calcium concentration in the diluted Gipshut
454 solution, the precipitation of Ca-uranates would be expected in the present study. However, the
455 solubility data given in literature were determined from undersaturation experiments, consistently
456 yielding lower equilibrium U(VI) concentrations compared to an oversaturation approach.
457 Furthermore, most solubility studies (e.g. (Altmaier et al., 2017)) were conducted over much longer
458 time spans, so that kinetics have to be considered. Under the given conditions, precipitation of
459 uranates might be a much slower process than U(VI) adsorption, making precipitation negligible
460 within the one-week sorption experiments. Tits and Wieland (2018) also found that at least up to
461 2×10^{-6} M U(VI) is stable in Ca-rich alkaline solutions for a time span of seven days. Having shown
462 that precipitation from the solution does not play a major role, surface-mediated precipitation
463 processes are still possible. Those could occur only when the Ca-bentonite is present, triggered by an
464 increased U(VI) concentration near the surface. In order to unambiguously distinguish between surface
465 precipitation and surface complexation, direct spectroscopic investigation of the U(VI) complexes
466 sorbed to the Ca-bentonite surface was necessary.

467

468 ## 3.5. U(VI) surface complexes studied with site-selective TRLFS

469 Figure 3a shows the excitation spectrum (black data points) of U(VI) sorbed on Ca-bentonite at pH 11
470 in the absence of CO_2 and a series of selected emission spectra (in color), obtained at different
471 excitation wavelengths. The excitation spectrum does not contain much spectral information. The
472 absence of distinct maxima is attributed to great variety of sorption sites within the sample, leading to

an inhomogeneous broadening. This heterogeneity of sorption sites is not surprising as Ca-bentonite is a very complex, multi-mineral material, where already montmorillonite can provide different complexation sites (e.g. edge sharing, corner sharing) and aluminol/silanol functionalities. The variety of sorption species can also be inferred from different emission spectra, which shift strongly, depending on the excitation energy. At low excitation wavelength (e.g. 472.8 nm) the emission spectra appear broadened and weakly resolved as the incident energy is high enough to excite all uranyl moieties within the sample. At higher excitation wavelengths (in Figure 3a exemplarily shown for λ_{ex} = 494.3, 499.7 and 505.2 nm), however, a clear luminescence line narrowing can be observed due to resonant/direct excitation of single species. The occurrence of luminescence line-narrowing alone already indicates the presence of adsorbed U(VI) surface complexes and eliminates U(VI) precipitation as predominant retention mechanism. In U(VI) precipitates, such as Na,Ca-uranates, the phenomenon of luminescence line narrowing is suppressed by homo-resonance energy transfer among the U-atoms arranged in close distance to each other, leading to a mutual excitation and consequently to a broadening of the signal (Lakowicz, 2006; Tits et al., 2015). Such signal broadening is observed in our batch sample prepared with an initial U(VI) concentration of 5×10^{-5} M to provoke U(VI) precipitation for comparison (Figure 3b). In fact, the obtained spectra show no luminescence line-narrowing, irrespective of the excitation energy. Broad and unresolved maxima around 545 nm appear at all excitation wavelengths, featuring luminescence lifetimes between 30 and 40 µs. Spectra with similar appearance and lifetimes have been identified as Ca-uranate in Tits et al. (2015) and Tits et al. (2011). No such features were observable in the sorption sample with 5×10^{-7} M uranium, implying that adsorption can be considered to be the only relevant retention mechanism at these experimental conditions.

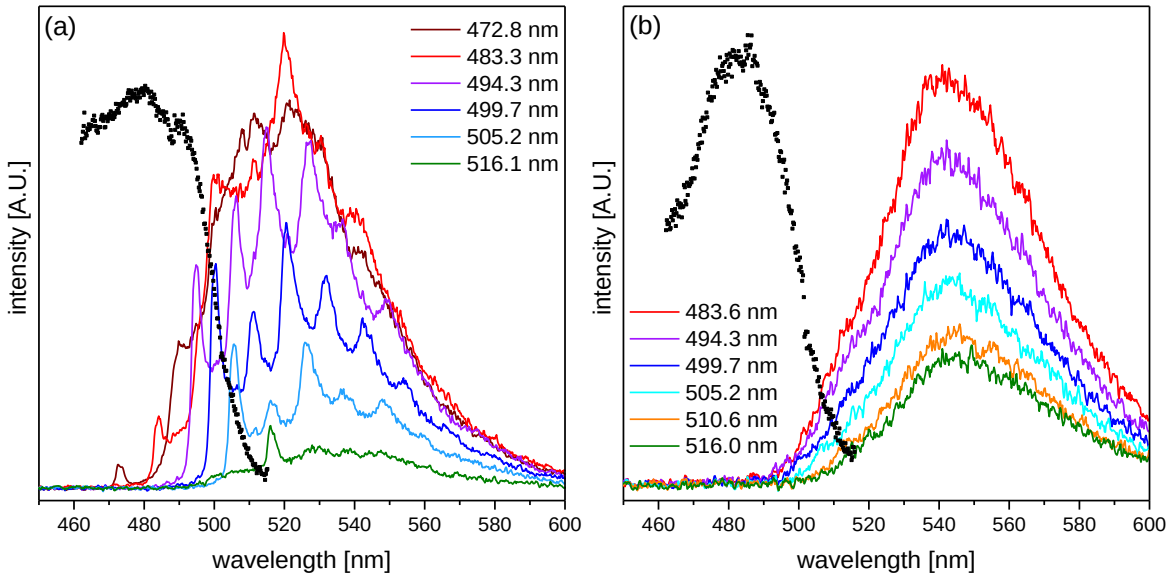

Figure 3: Excitation (black dots) and emission spectra (colored lines) of U(VI) sorbed on Ca-bentonite in the absence of CO_2 at pH 11 with [U(VI)] = 5×10^{-7} M (a) and [U(VI)] = 5×10^{-5} M (b) obtained with site-selective TRLFS at 10 K.

From the absolute positions of the narrowed peaks of the emission spectra alone, not much information about the U(VI) surface speciation can be deduced. However, the relative position of the maxima (i.e. the distance of the different electronic and vibronic transition lines) provides insight into the structure of the uranyl unit. For that purpose, electronic and vibronic transition events were assigned to the single emission lines, exemplarily shown for the emission spectrum obtained at 499.7 nm excitation wavelength (Figure 4). In phase with the incident laser energy, the resonant electronic transition line E_1 appears, followed by the lines of vibronic progression on E_1 ($S_{1,E1}$ and $S_{2,E1}$) caused by the vibronic degeneracy of the electronic ground state. Furthermore, a second (non-resonant) U(VI) species with the non-resonant electronic transition line E_2 can be identified. Also this species is superimposed by the first two lines of vibronic progression ($S_{1,E2}$ and $S_{2,E2}$). As already discussed in section 2.4, the spacing between the first two peaks of each species (i.e. between E_1 and $S_{1,E1}$ and between E_2 and $S_{1,E2}$, respectively) corresponds to the total symmetric stretch vibration (ν_s) of the uranyl cation in the ground state. The spacing of the first (resonantly excited) species $\nu_s(1)$ is 781 ± 5 cm^{-1} (Table 3). With 758 ± 12 cm^{-1}, the stretch vibration $\nu_s(2)$ of the second, non-resonantly excited, species noticeably differs from the first one. Both frequencies lie in the typical range for U(VI) minerals and sorbed species (Wang et al., 2011; Wang et al., 2005), and are significantly

514 smaller than values found for aqueous species (Nguyen-Trung et al., 2000), such as $UO_2(OH)_3^-$, which
515 is dominating the aqueous speciation at pH 11 (Table 3). Especially for species 2, this strong
516 weakening of the axial U-O bond implies strong bonding in the U(VI) equatorial plane upon
517 adsorption (i.e. inner-sphere surface complexation). The comparatively higher frequency for species 1
518 could then hint towards outer-sphere sorption.

519 Inner-sphere surface complexation of U(VI) at montmorillonite silanol and aluminol edge sites has
520 been previously demonstrated at neutral pH by TRLFS (Chisholm-Brause et al., 2004; Chisholm-
521 Brause et al., 2001; Kowal-Fouchard et al., 2004) and EXAFS (Catalano and Brown, 2005; Marques
522 Fernandes et al., 2012). Between pH 8 and 13, no spectroscopic studies dealing with U(VI) surface
523 complexation exist for comparison. The present study suggests that inner-sphere surface complexation
524 at pH 10-12 can occur in a similar way as at neutral pH. A couple of studies are available on U(VI)
525 sorption by cementitious systems above pH 13. The total symmetric stretch vibration of species 2 of
526 the present study compares very well to that of a surface complex detected on C-S-H phases at pH
527 13.3 by Tits et al. (2015). As $UO_2(OH)_3^-$ is the dominant aqueous U(VI) species at pH 11, electrostatic
528 repulsion does not seem to prevent this anionic complex from adsorbing to the negatively charged clay
529 surface. A possible role of cations (i.e. Ca^{2+}) mediating between the anionic hydrolysis complex and
530 the mineral surface will be discussed below.

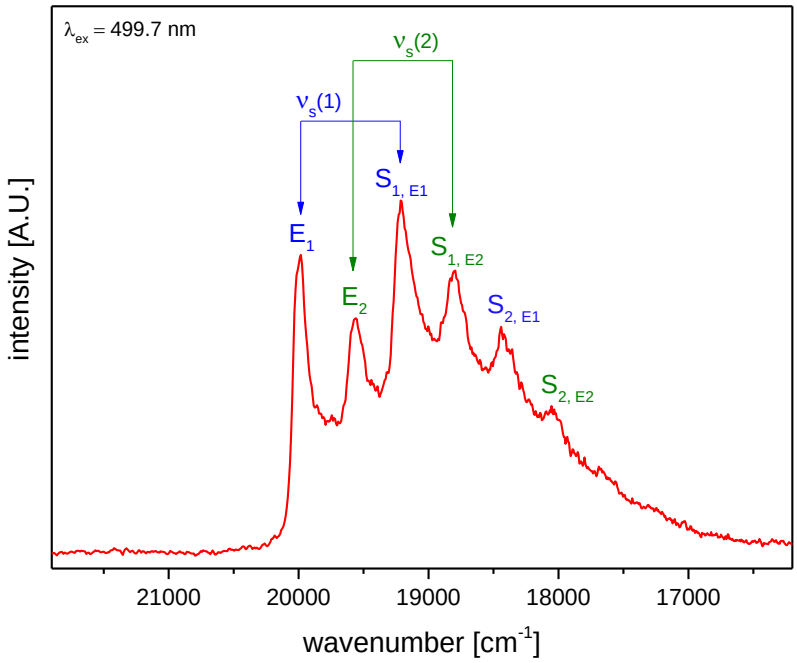

Figure 4: Luminescence emission spectrum of 5×10^{-7} M U(VI) sorbed on Ca-bentonite at pH 11 in the absence of CO_2 after laser excitation at 499.7 nm. Two U(VI) species could be identified based on their different electronic and vibronic transitions assigned with blue and green letters for species 1 and species 2, respectively. Spacing between the first two main peaks of each species $\nu_s(1)$ and $\nu_s(2)$ are indicated.

Table 3: Frequencies of the total symmetric stretch vibration (ν_s) deduced from the spacing between the luminescence emission lines of U(VI) (5×10^{-7} M) sorbed on Ca-bentonite at pH 11 in comparison to literature values.

Uranyl species	ν_s [cm^{-1}]	Reference
1	781 ± 5	this study
2	758 ± 12	this study
UO_2^{2+}	870	Nguyen-Trung et al. (2000)
$UO_2(OH)_3^-$	804	Nguyen-Trung et al. (2000)
U(VI) minerals and sorbed species	700-800	Wang et al. (2011); Wang et al. (2005)
Adsorbed on C-S-H	758	Tits et al. (2015)

3.6. Local U(VI) coordination environment studied with EXAFS

Figure 5 shows the EXAFS spectra and Fourier transforms (FT) of the sorption samples with different pH and carbonate concentrations (N_2, LC, HC), including a reference spectrum of the aqueous $UO_2(OH)_4^{2-}$ complex. None of the spectra shows indications for U(VI) precipitation (i.e. no U-U backscattering paths detected). Consequently, as already deduced from site-selective TRLFS, the predominant retention mechanism of U(VI) in Ca-bentonite under the given conditions is adsorption.

A trend of decreasing average equatorial oxygen (O_{eq}) distance with increasing pH is observed within each sample series. While the peaks for O_{eq} and axial oxygen (O_{ax}) are clearly separated at pH 8 and 9, at elevated pH only combined peaks for O_{eq} and O_{ax} can be observed in the Fourier transforms (FT).

The application of ITFA (Text SM2) showed that all ten EXAFS spectra can be reproduced with two spectral components (Figure 5). Consequently, two structurally different sorption complexes are present in the system with different fractions in each sample, depending on the pH. According to the result of the iterative target test (ITT) component 1 is predominant at the lowest pH of each sample set (i.e. sample 1 (N_2, pH 8.0) or sample 5 (LC, pH 9)) and occurs independently of the presence or absence of carbonate. Conversely, the fraction of component 2 is highest in the samples prepared at high pH (Figure 6). According to the extracted single component spectra and the results of the ITFA, component 2 matches to the $UO_2(OH)_4^{2-}$ reference. Hence, for the samples with high pH, both the spectrum and the local atomic structure around U(VI) agree with those of the aqueous $UO_2(OH)_4^{2-}$ complex. Consequently, component 2 is a sorption species at the bentonite surface with a structure similar to the aqueous $UO_2(OH)_4^{2-}$ complex.

An interaction of U(VI) with carbonate would lead to the detection of a third component in the sample series LC and HC. However, only two components were detected. Consequently, no ternary U(VI) carbonate sorption complexes are present on the Ca-bentonite surface. This observation is in accordance with the work of Marques Fernandes et al. (2012), where no influence of carbonate on the surface complexation could be detected with EXAFS, also supporting the hypothesis of Tournassat et al. (2018) that uranyl carbonate complexes do not adsorb on montmorillonite surfaces to significant amounts.

We performed a shell fit of the ITT isolated spectrum of component 1 and of the spectrum of the aqueous $UO_2(OH)_4^{2-}$ complex, while the latter was selected instead of the ITT isolated spectrum of component 2 in order to gain a higher resolution for the determination of radial distances due to the larger available *k*-range. The fit of the spectra and the corresponding EXAFS structural parameters are given in Figure 7 and Table 4.

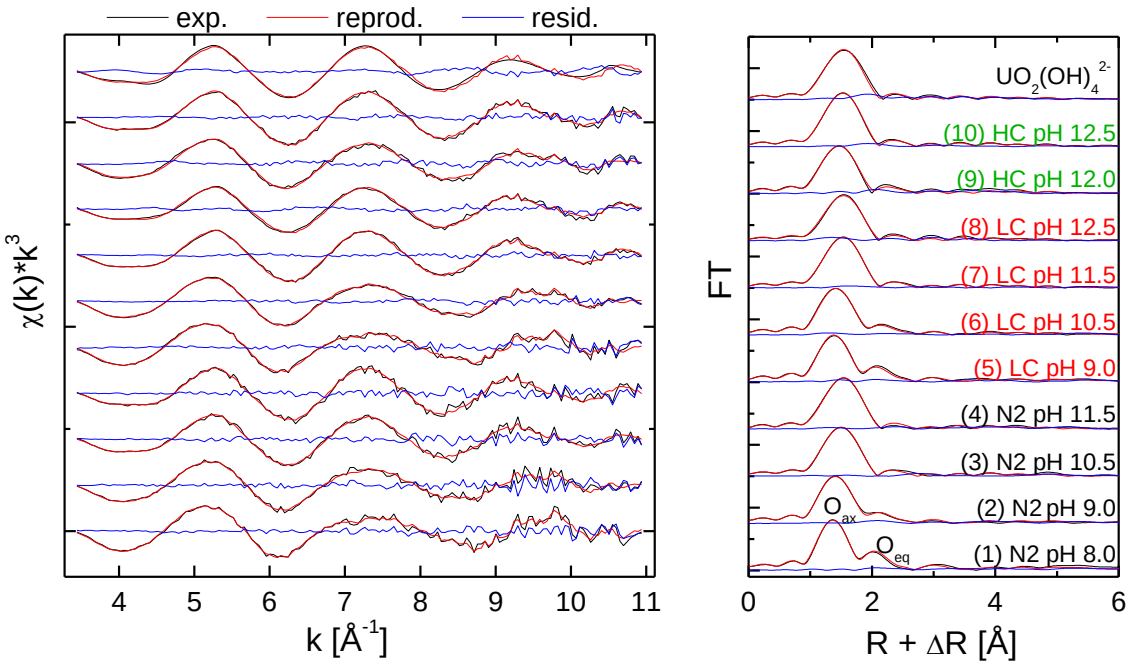

571

572 *Figure 5: U L_{III}-edge EXAFS spectra (left, black) and corresponding Fourier transforms (right, black) with reproductions*
573 *(red) and the residual (blue) of U(VI) sorption samples on Ca-bentonite in the absence of carbonate (N_2) and at low (LC) and*
574 *high (HC) carbonate concentrations, including a reference spectrum of the aqueous $UO_2(OH)_4^{2-}$ complex (Moll et al., 2014).*

575

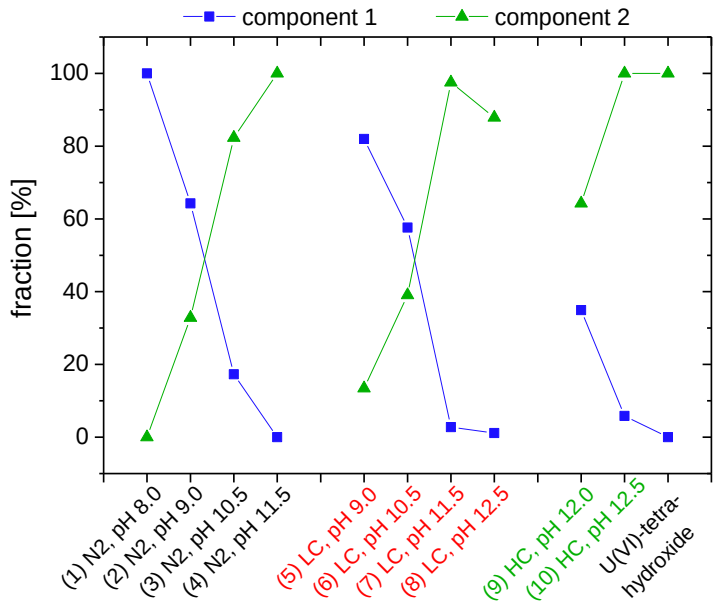

576

577 *Figure 6: ITT calculated fractions of component 1 and component 2 for U(VI) sorption samples on Ca-bentonite in the*
578 *absence of carbonate (N_2) and at low (LC) and high (HC) carbonate concentration, including the reference of the aqueous*
579 *$UO_2(OH)_4^{2-}$ complex (Moll et al., 2014).*

580

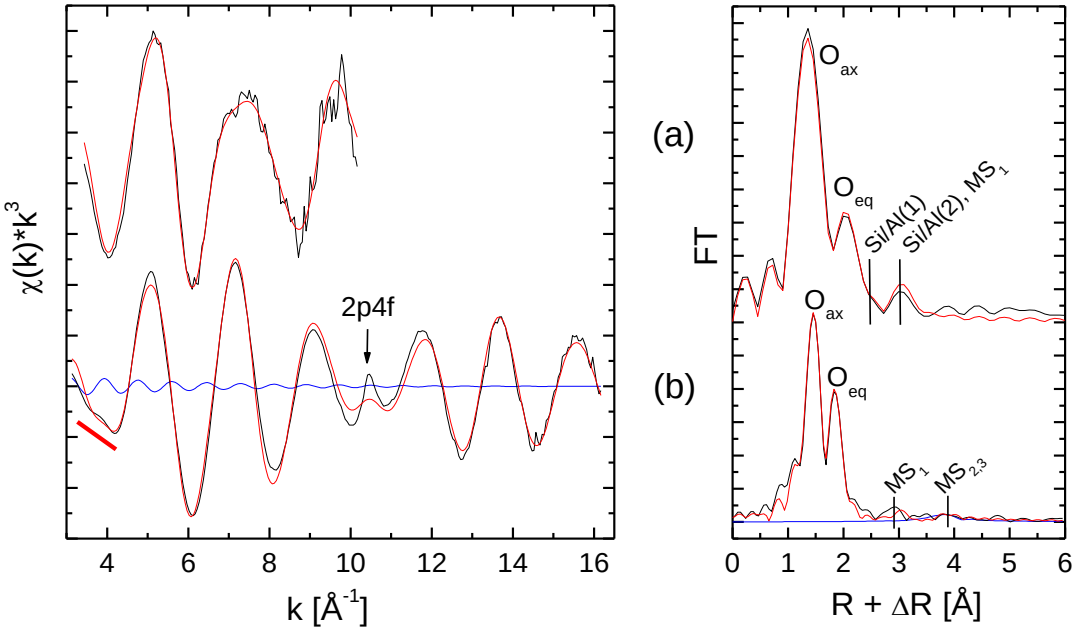

581

582 *Figure 7: U L_{III}-edge EXAFS spectra of the ITFA isolated component 1 (a) and of the aqueous $UO_2(OH)_4^{2-}$ complex (b) (left)*
583 *with corresponding Fourier transforms (FT) (right) together with the shell fit (red). Spectral contribution of MS_2 and MS_3*
584 *(blue). 2p4f multi-electron excitation assigned with arrow (Hennig, 2007).*

585 For component 1 we obtained an equatorial oxygen shell (U-O_{eq}) at a distance of ~2.38 Å (*CN* fixed
586 to 5). This shortened distance in comparison to U-O_{eq} of hydrated outer-sphere sorption complexes on
587 montmorillonite described in literature of ~2.43 Å ((Chisholm-Brause et al., 1994; Sylwester et al.,
588 2000)) suggests the formation of inner-sphere surface complexes. Marques Fernandes et al. (2012)
589 observed a splitting of the equatorial oxygen shell in sorption samples at pH 8 and obtained U-O_{eq}
590 distances of ~2.3 Å and ~2.48 Å. Such a splitting cannot be resolved in the present study due to lower
591 resolution in radial distances. However, when averaging the reported distances of Marques Fernandes
592 et al. (2012), weighted by the coordination numbers (3.1 and 2.9), a mean U-O_{eq} distance of 2.387 Å
593 can be derived, which is in excellent agreement with our results. Furthermore, two Si/Al shells could
594 be fitted in radial distances of 3.11 Å and 3.32 Å. Those are in good agreement with the Si/Al
595 distances of 3.09 Å and 3.28 Å for the bidentate inner-sphere sorption complexes on montmorillonite
596 at pH 8 described by Marques Fernandes et al. (2012). Therefore, the same type of U(VI) surface
597 complex is proposed for our component 1.

598 Representative for component 2, the high symmetry of the $UO_2(OH)_4^{2-}$ complex leads to the
599 appearance of a spectral feature at k = 3.5 – 4.3 $Å^{-1}$ (Figure 7, highlighted with red line) which
600 originates from the multiple scattering (MS) paths MS_2 ($U\text{-}O_{eq(1)}\text{-}U\text{-}O_{eq(2)}$) and MS_3 ($U\text{-}O_{eq(1)}\text{-}U\text{-}O_{eq(1)}$)
601 (Figure SM4). The scattering contribution of these inherent MS paths is strongly enhanced due to the
602 linear arrangement of the involved atoms, comparable with the arrangement in the linear "yl" chain of
603 U(VI) for which the MS_1 ($U\text{-}O_{ax(1)}\text{-}U\text{-}O_{ax(2)}$) shows a significant spectral contribution. Note that we
604 also tested the 4-fold degenerated 3-legged MS path $U\text{-}O_{eq(1)}\text{-}O_{eq(2)}$, but no further improvement of the
605 fit was obtained. The sum of the MS_2 and MS_3 scattering contributions causes a truncation of the
606 negative maximum of the EXAFS oscillation in this k-region (Figure 7). The distance of 4.55 Å
607 measured for MS_2 and MS_3 matches, within the common error in determination of distances probed by
608 EXAFS (Li et al., 1995), the theoretically expected distance of 4.54 Å which would be twice the O_{eq}
609 distance of 2.27 Å (Table 4). The O_{ax} and O_{eq} distances and the corresponding Debye-Waller factors
610 (σ^2) are in good agreement with published data (Table 4) where the MS feature was not explored so
611 that only the coordination number (*CN*) and/or the O_{eq} distance could be used for the structural
612 interpretation of the aqueous $UO_2(OH)_4^{2-}$ complex (Moll et al., 2000; Moll et al., 2014). However, the
613 error in determination of the *CN* is approximately 20 % (Li et al., 1995), hence the EXAFS determined
614 *CN* is not reliable enough to be used as a proof for the presence of a 4-fold coordinated U(VI)
615 complex. Thus, only the presence of the MS feature at k = 3.5 – 4.3 $Å^{-1}$ indicates univocally a
616 symmetric 4-fold coordination of U(VI). Due to the appearance at low k-values, the MS feature is
617 visible in the X-ray absorption near edge structure (XANES) at 17240 eV. Therefore, XANES can be
618 also used for the identification of a 4-fold coordination, as exemplary shown for the aqueous
619 complexes of the 5- and 4-fold coordinated U(VI)-hydrate ($UO_2(H_2O)_5^{2+}$) and $UO_2(OH)_4^{2-}$,
620 respectively (Figure SM11).

621 The MS feature at k = 3.5 – 4.3 $Å^{-1}$ is also present in case of the high pH sorption samples (Figure 5),
622 which is in line with the ITFA result (Figure 6) pointing to the prevalence of a sorption complex with
623 an $UO_2(OH)_4^{2-}$ like structure. In the case of 5-fold coordinated U(VI) the $O_{eq(1)}\text{-}U\text{-}O_{eq(2)}$ angles are not
624 straight, so that the spectral contribution of MS_2 and MS_3 diminishes as observed for component 1

625 which covers the lower pH sorption samples. Thus, beside the fractions of the two sorption complexes
626 the ITT shows also the transition from a 5-fold to a 4-fold coordination of U(VI) with increasing pH.

627

628 *Table 4: Shell fit EXAFS structural parameters for component 1 and the aqueous $UO_2(OH)_4^{2-}$ complex.*

Shell	*CN*	*R* / Å	σ^2 / Å^2	ΔE_0 / eV
		Component 1		
O_{ax}	2*	1.797(3)	0.0010(2)	11.0(5)
MS_1	/2	/3.594	/0.002	/11.0
O_{eq}	5*	2.382(8)	0.0154(8)	/11.0
Si/Al(1)	1.5(2)	3.11(1)	0.003[a]	/11.0
Si/Al(2)	1.2(2)	3.32(1)	0.003[a]	/11.0
		aqueous $UO_2(OH)_4^{2-}$ complex		
O_{ax}	2*	1.8254(9)	0.00176(6)	3.6(3)
		1.83[b], 1.82[c]	0.001[b], 0.0015[c]	
MS_1	/2	/3.6508	/0.00352	/3.6
O_{eq}	4*	2.271(1)	0.0040(1)	/3.6
		2.25[b],	0.0043[b],	
		2.26[b], 2.27[c]	0.0046[b], 0.004[c]	
MS_2	/4	4.55(2)	0.005(3)	/3.6
MS_3	/4	/4.55	/0.005	/3.6

629 * - fixed parameter, / - linked parameter, *CN* − coordination number, *R* − radial distance, σ^2 − Debye-Waller factor, ΔE_0 − shift in energy
630 threshold. The standard deviation of the fitted parameters is given in parentheses. Amplitude reduction factor $S_0^2 = 1.0$. Multiple scattering
631 paths MS_1 (U-$O_{ax(1)}$-U-$O_{ax(2)}$), MS_2 (U-$O_{eq(1)}$-U-$O_{eq(2)}$), MS_3 (U-$O_{eq(1)}$-U-$O_{eq(1)}$). [a] - σ^2 fixed at value taken from literature (Hennig et al., 2002;
632 Marques Fernandes et al., 2012), [b] - (Moll et al., 2000), [c] - (Moll et al., 2014).

633 Despite the strong similarity with the aqueous $UO_2(OH)_4^{2-}$ complex according to the shell fit, it can be
634 ruled out that component 2 corresponds to an aqueous species, as U(VI) was almost completely
635 removed from solution and the EXAFS samples were prepared as wet pastes with only a minor

amount of aqueous solution present. An aqueous species could therefore be present in the samples only as a minor fraction, while component 2 accounts for up to 100 % in some of the samples. Consequently, component 2 can definitely be assigned to an adsorbed species. Furthermore, $UO_2(OH)_4^{2-}$ is expected to be the dominant aqueous species only at pH > 12, as confirmed by our TRLFS measurements. In our EXAFS samples between pH 10 and 12, $UO_2(OH)_3^-$ is the dominant aqueous species prior to sorption. Owing to the difficulty to obtain $UO_2(OH)_3^-$ as a single, isolated species, no EXAFS reference spectra exist for this complex. Its structure, especially the coordination number of equatorial oxygen, is not clarified. While sometimes referred to be 5-fold coordinated (3 OH and 2 H_2O), the DFT study of Ingram et al. (2006) proposed a 4-fold coordination (3 OH and 1 H_2O). Our finding of a 4-fold coordination of component 2 supports this hypothesis. Apparently, this geometry is then preserved upon sorption, indicating relatively weak interaction with the substrate. Also the fact that it was not possible to fit U-Si/Al scattering paths for component 2 indicates a larger distance to the mineral surface. The complex could be bound via mediating cations such as Ca^{2+}, located between the negatively charged surface and the anionic uranyl hydroxide unit. Evidence for Ca^{2+} attachment on the bentonite surface can be seen in our zeta potential measurements, where a significant increase of the zeta potential was observed in the presence of Ca^{2+} (Figure SM7). Thus, the sorption of negatively charged uranyl species would be realized by initial adsorption of Ca^{2+} to the clay mineral surface (Gascó and Méndez, 2005; Missana and García-Gutiérrez, 2007; Pointeau et al., 2004; Viallis-Terrisse et al., 2001), leading to a local charge inversion and facilitating attachment of anionic uranyl hydroxides. Also the formation of aqueous ternary Ca-uranyl-hydroxides is possible, which would have a neutral or even positive net charge and would be therefore capable of interacting with the negatively charged bentonite surface. The existence of such ternary Ca-uranyl-hydroxide complexes at (hyper)alkaline conditions is hypothesized but has not been explored yet in detail.

Based on the knowledge obtained from EXAFS, also an assignment of the two species detected with site-selective TRLFS to the structurally different surface complexes is possible. Assuming a $UO_2(OH)_4^{2-}$ like structure for component 2, a theoretical frequency for the symmetric stretch vibration can be calculated according to an empirical relationship for aqueous uranyl hydroxide complexes found by Nguyen-Trung et al. (2000). With four equatorial oxygens a ν_s of 782 cm^{-1} is obtained, which

is almost identical to the ν_s of TRLFS-species 1 (781 cm^{-1}, Table 3). Accordingly, TRLFS-species 2, with a lower ν_s of 758 cm^{-1}, has to correspond to the 5 fold-coordinated bidentate surface complex (EXAFS-component 1). This assumption is reasonable as a decrease of ν_s (as a consequence of a weakening of the axial U-O bonds) is a response to an increased electron density and increased ligand bond strength in the equatorial plane (Di Pietro and Kerridge, 2016; McGlynn et al., 1961; Nguyen-Trung et al., 2000; Tsushima, 2011). For EXAFS-component 1 this is a result of the bidentate binding and the close proximity to substrate atoms (Si/Al) in contrast to EXAFS-component 2, where no backscattering contributions from the substrate could be detected. Due to extensive σ donation from the surface, Tsushima et al. (1998) and Morris et al. (1994) obtained similar values for ν_s for inner-sphere surface complexes on silver nanoparticles (750 cm^{-1}) and smectite edge sites (751 cm^{-1}), respectively.

4. Conclusions

Sorption experiments demonstrated that U(VI) retention on Ca-bentonite in the pH range 8-13 can be very efficient, also in the presence of carbonate. Above a certain pH, which is determined by the carbonate concentration, carbonate does not play a role in the U(VI) complexation in solution anymore due to the dominance of hydrolysis. A clear correlation between sorption behavior and aqueous U(VI) speciation in the diluted Gipshut solution was observed with TRLFS conducted at 153 K. Retention reaches a maximum at conditions where $UO_2(OH)_3^-$ is the predominant aqueous species. Solubility tests have shown that the observed complete U(VI) removal at pH 10-12 cannot be attributed to precipitation of (earth) alkali-uranates from the solution. In order to unambiguously distinguish between surface precipitation and surface complexation as dominant retention mechanism, direct spectroscopic investigations of the U(VI) complexes on the Ca-bentonite surface were performed with site-selective TRLFS (at 10 K) and EXAFS. The occurrence of luminescence line narrowing and the frequency of the total symmetric stretch vibration obtained from the TRLFS emission spectra, indicate the presence of two U(VI) surface complexes. Also EXAFS spectra showed no indication of U(VI) precipitation. With increasing pH, the nature of the retained U(VI) complexes shifts from inner-sphere surface complexes with an overall equatorial coordination of five adsorbed on aluminol or silanol edge sites to surface complexes with a 4-fold equatorial coordination which are presumably bound to the surface via mediating cations (i.e. Ca^{2+}). For the first time, a 4-fold coordination in the equatorial plane of U(VI) was univocally proven with the help of a multiple scattering feature originating from the strong symmetry of the complexes, and without the need for error-prone shell fitting.

Consequently, by the combination of different spectroscopic methods, surface complexation was unequivocally identified as the responsible process for the strong U(VI) retention by Ca-bentonite at (hyper)alkaline conditions and low U(VI) concentrations. That means, that under certain alkaline repository conditions, where precipitation of uranates does not occur (due to very low concentrations or kinetic restraints), uranium is still effectively retained in argillaceous media by adsorption of negatively charged metal complexes. The affinity towards the formation of surface complexes, possibly by contribution of mediating cations such as Ca^{2+}, overrules the repulsive electrostatic forces

between the anionic aqueous complex and the negatively charged clay surface. This finding is of great relevance, as also the migration of very small amounts of U(VI) out of waste repositories could lead to a hazardous accumulation in the anthroposphere in the long term.

Acknowledgements

This work was funded by the Federal Ministry for Economic Affairs and Energy (BMWi) within the framework of the project GRaZ (No. 02 E 11415B). The authors would like to thank Atsushi Ikeda-Ohno for support with PXRD measurements, Sabrina Beutner and Birke Pfützner for ICP-MS measurements, Carola Eckardt for determination of DIC and BET, Frank Bok for calculation of aqueous U(VI) speciation, Stephan Weiss for assistance with PCS and zeta potential measurements, Klaus Meier (Helmholtz-Institut Freiberg für Ressourcentechnologie) for laser granulometry, Paul Dullies for contribution to the leaching results and Vinzenz Brendler and Robin Steudtner for intensive discussion.

Appendix A. Supplementary material

Supplementary data to this article can be found online at …

References

Altmaier M, Metz V, Neck V, Müller R, Fanghänel T. Solid-liquid equilibria of $Mg(OH)_{2(cr)}$ and $Mg_2(OH)_3Cl{\cdot}4H_2O_{(cr)}$ in the system Mg-Na-H-OH-Cl-H_2O at 25°C. Geochim. Cosmochim. Acta 2003; 67: 3595-3601.

Altmaier M, Yalçıntaş E, Gaona X, Neck V, Müller R, Schlieker M, Fanghänel T. Solubility of U(VI) in chloride solutions. I. The stable oxides/hydroxides in NaCl systems, solubility products, hydrolysis constants and SIT coefficients. J. Chem. Thermodyn. 2017; 114: 2-13.

Ankudinov AL, Ravel B, Rehr JJ, Conradson SD. Real-space multiple-scattering calculation and interpretation of X-ray-absorption near-edge structure. Phys. Rev. B 1998; 58: 7565-7576.

Bachmaf S, Planer-Friedrich B, Merkel BJ. Effect of sulfate, carbonate, and phosphate on the uranium(VI) sorption behavior onto bentonite. Radiochim. Acta 2008; 96: 359-366.

Berner UR. Evolution of pore water chemistry during degradation of cement in a radioactive waste repository environment. Waste Manag 1992; 12: 201-219.

Bernhard G, Geipel G, Reich T, Brendler V, Amayri S, Nitsche H. Uranyl(VI) carbonate complex formation: Validation of the $Ca_2UO_2(CO_3)_{3(aq.)}$ species. Radiochim. Acta 2001; 89: 511-518.

Bots P, Morris K, Hibberd R, Law GT, Mosselmans JF, Brown AP, Doutch J, Smith AJ, Shaw S. Formation of stable uranium(VI) colloidal nanoparticles in conditions relevant to radioactive waste disposal. Langmuir 2014; 30: 14396-14405.

Catalano JG, Brown GE. Uranyl adsorption onto montmorillonite: Evaluation of binding sites and carbonate complexation. Geochim. Cosmochim. Acta 2005; 69: 2995-3005.

Chisholm-Brause C, Conradson SD, Buscher CT, Eller PG, Morris DE. Speciation of uranyl sorbed at multiple binding sites on montmorillonite. Geochim. Cosmochim. Acta 1994; 58: 3625-3631.

Chisholm-Brause CJ, Berg JM, Little KM, Matzner RA, Morris DE. Uranyl sorption by smectites: spectroscopic assessment of thermodynamic modeling. J Colloid Interface Sci 2004; 277: 366-382.

Chisholm-Brause CJ, Berg JM, Matzner RA, Morris DE. Uranium(VI) Sorption Complexes on Montmorillonite as a Function of Solution Chemistry. J Colloid Interface Sci 2001; 233: 38-49.

Di Pietro P, Kerridge A. U-Oyl Stretching Vibrations as a Quantitative Measure of the Equatorial Bond Covalency in Uranyl Complexes: A Quantum-Chemical Investigation. Inorg Chem 2016; 55: 573-583.

Drobot B, Bauer A, Steudtner R, Tsushima S, Bok F, Patzschke M, Raff J, Brendler V. Speciation Studies of Metals in Trace Concentrations: The Mononuclear Uranyl(VI) Hydroxo Complexes. Anal Chem 2016; 88: 3548-3555.

Fernández R, Mäder U, Rodríguez M, Virgil de la Villa R, Cuevas J. Alteration of compacted bentonite by diffusion of highly alkaline solutions. Eur J Mineral 2009; 21: 725-735.

758 Fritsch K. Investigation of uranium(VI) retention by montmorillonite at high ionic strengths.
759 Doctoral Thesis. Technische Universität Dresden, Dresden, Germany, 2018.

760 Gascó G, Méndez A. Sorption of Ca^{2+}, Mg^{2+}, Na^{+} and K^{+} by clay minerals. Desalination 2005; 182:
761 333-338.

762 Gaucher ÉC, Blanc P, Bardot F, Braibant G, Buschaert S, Crouzet C, Gautier A, Girard J-P, Jacquot
763 E, Lassin A, Negrel G, Tournassat C, Vinsot A, Altmann S. Modelling the porewater
764 chemistry of the Callovian–Oxfordian formation at a regional scale. Comptes Rendus
765 Geoscience 2006; 338: 917-930.

766 George GN, Pickering IJ. EXAFSPAK: A Suite of Computer Programs for Analysis of X-ray
767 Absorption Spectra, Stanford Synchrotron Radiation Laboratory, Stanford, CA. USA.,
768 1995.

769 Guillaumont R, Fanghänel T, Fuger J, Grenthe I, Neck V, Palmer DA, Rand MH. Update on the
770 Chemical Thermodynamics of Uranium, Neptunium, Plutonium, Americium and
771 Technetium. Amsterdam, The Netherlands: Elsevier, 2003.

772 Hama K, Kunimaru T, Metcalfe R, Martin AJ. The hydrogeochemistry of argillaceous rock
773 formations at the Horonobe URL site, Japan. Phys Chem Earth 2007; 32: 170-180.

774 Harfouche M, Wieland E, Dähn R, Fujita T, Tits J, Kunz D, Tsukamoto M. EXAFS study of U(VI)
775 uptake by calcium silicate hydrates. J Colloid Interface Sci 2006; 303: 195-204.

776 Hennig C. Evidence for double-electron excitations in the L-3-edge X-ray absorption spectra of
777 actinides. Phys. Rev. B 2007; 75: 1-7.

778 Hennig C, Reich T, Dähn R, Scheidegger AM. Structure of uranium sorption complexes at
779 montmorillonite edge sites. Radiochim. Acta 2002; 90: 653-657.

780 Ingram KI, Haller LJ, Kaltsoyannis N. Density functional theory investigation of the geometric
781 and electronic structures of $[UO_2(H_2O)m(OH)n](2 - n)$ (n + m = 5). Dalton Trans 2006:
782 2403-2414.

783 Joseph C, Stockmann M, Schmeide K, Sachs S, Brendler V, Bernhard G. Sorption of U(VI) onto
784 Opalinus Clay: Effects of pH and humic acid. Appl Geochem 2013; 36: 104-117.

785 Kaplan DI, Gervais TL, Krupka KM. Uranium(VI) Sorption to Sediments Under High pH and Ionic
786 Strength Conditions. Radiochim. Acta 1998; 80: 201-211.

787 Kenney JPL, Kirby ME, Cuadros J, Weiss DJ. A conceptual model to predict uranium removal from
788 aqueous solutions in water–rock systems associated with low- and intermediate-level
789 radioactive waste disposal. RSC Adv. 2017; 7: 7876-7884.

790 Kitamura A, Yamamura T, Haseb H, Yamamoto T, Moriyama H. Measurement of Hydrolysis
791 Species of U(VI) by Time-Resolved Laser Induced Fluorescence Spectroscopy.
792 Radiochim. Acta 1998; 82: 147-152.

793 Kowal-Fouchard A, Drot R, Simoni E, Ehrhardt J. Use of Spectroscopic Techniques for
794 Uranium(VI)/Montmorillonite Interaction Modeling. Environ. Sci. Technol 2004; 38:
795 1399-1407.

796 Lakowicz JR. Principles of fluorescence spectroscopy. New York: Springer, 2006.

Lee J-Y, Vespa M, Gaona X, Dardenne K, Rothe J, Rabung T, Altmaier M, Yun J-I. Formation, stability and structural characterization of ternary $MgUO_2(CO_3)_3^{2-}$ and $Mg_2UO_2(CO_3)_{3(aq)}$ complexes. Radiochim. Acta 2017; 105: 171–185.

Lee JY, Yun JI. Formation of ternary $CaUO_2(CO_3)_3^{(2-)}$ and $Ca_2UO_2(CO_3)_{3(aq)}$ complexes under neutral to weakly alkaline conditions. Dalton Trans 2013; 42: 9862-9869.

Li GG, Bridges F, Booth CH. X-ray-absorption fine-structure standards: A comparison of experiment and theory. Phys Rev B Condens Matter 1995; 52: 6332-6348.

Lommerzheim M, Jobmann A. Endlagerkonzept sowie Verfüll- und Verschlusskonzept für das Standortmodell NORD. TEC-08-2014-Z. DBE Technology, 2014.

Macé N, Wieland E, Dähn R, Tits J, Scheinost AC. EXAFS investigation on U(VI) immobilization in hardened cement paste: influence of experimental conditions on speciation. Radiochim. Acta 2013; 101: 379-389.

Maher K, Bargar JR, Brown GE, Jr. Environmental speciation of actinides. Inorg Chem 2013; 52: 3510-3532.

Marques Fernandes M, Baeyens B, Dähn R, Scheinost AC, Bradbury MH. U(VI) sorption on montmorillonite in the absence and presence of carbonate: A macroscopic and microscopic study. Geochim. Cosmochim. Acta 2012; 93: 262-277.

Martínez-Torrents A, Meca S, Baumann N, Martí V, Giménez J, de Pablo J, Casas I. Uranium speciation studies at alkaline pH and in the presence of hydrogen peroxide using time-resolved laser-induced fluorescence spectroscopy. Polyhedron 2013; 55: 92-101.

Matz W, Schell N, Bernhard G, Prokert F, Reich T, Claussner J, Oehme W, Schlenk R, Dienel S, Funke H, Eichhorn F, Betzl M, Prohl D, Strauch U, Hüttig G, Krug H, Neumann W, Brendler V, Reichel P, Denecke MA, Nitsche H. ROBL - a CRG beamline for radiochemistry and materials research at the ESRF. J. Synchrotron Radiat 1999; 6: 1076-1085.

Mazurek M. Long-term Used Nuclear Fuel Waste Management – Geoscientific Review of the Sedimentary Sequence in Southern Ontario. Institute of Geological Sciences, University of Bern Bern, Switzerland, 2004.

McGlynn SP, Smith JK, Neely WC. Electronic Structure, Spectra, and Magnetic Properties of Oxycations. III. Ligation Effects on the Infrared Spectrum of the Uranyl Ion J. Chem. Phys. 1961; 35: 105-116.

Meleshyn A, Azeroual M, Reeck T, Houben G, Riebe B, Bunnenberg C. Influence of (Calcium-)Uranyl-Carbonate Complexation on U(VI) Sorption on Ca- and Na-Bentonites. Environ. Sci. Technol 2009; 43: 4896–4901.

Milodowski AE, Norris S, Alexander WR. Minimal alteration of montmorillonite following long-term interaction with natural alkaline groundwater: Implications for geological disposal of radioactive waste. Appl Geochem 2016; 66: 184-197.

Missana T, García-Gutiérrez M. Adsorption of bivalent ions (Ca(II), Sr(II) and Co(II)) onto FEBEX bentonite. Phys Chem Earth 2007; 32: 559-567.

Moll H, Reich T, Szabo Z. The hydrolysis of dioxouranium(VI) investigated using EXAFS and O-17-NMR. Radiochim. Acta 2000; 88: 411-415.

837 Moll H, Rossberg A, Steudtner R, Drobot B, Mueller K, Tsushima S. Uranium(VI) Chemistry in
838 Strong Alkaline Solution: Speciation and Oxygen Exchange Mechanism. Inorg. Chem.
839 2014; 53: 1585-1593.

840 Moroni LP, Glasser FP. Reactions between cement components and U(VI) oxide. Waste Manag
841 1995; 15: 243-254.

842 Morris DE, Conradson SG, Chisholm-Brause CJ, Barr ME, Eller PG. Optical spectroscopic studies
843 of the sorption of UO_2^{2+} species on a reference smectite. Geochim. Cosmochim. Acta
844 1994; 58: 3613-3623.

845 Moulin C, Laszak I, Moulin V, Tondre C. Time-Resolved Laser-Induced Fluorescence as a Unique
846 Tool for Low-Level Uranium Speciation. Appl. Spectrosc. 1998; 52: 528-535.

847 Nguyen-Trung C, Palmer DA, Begun GM, Peiffert C, Mesmer RE. Aqueous Uranyl Complexes 1.
848 Raman Spectroscopic Study of the Hydrolysis of Uranyl(VI) in Solutions of
849 Trifluoromethanesulfonic Acid and/or Tetramethylammonium Hydroxide at 25°C and
850 0.1 MPa. J Solution Chem 2000; 29: 101-129.

851 Nowak T, Maßmann J. Endlagerstandortmodell Nord (AnSichT) - Teil III: Auswahl von Gesteins-
852 und Fluideigenschaften für numerische Modellberechnungen im Rahmen des
853 Langzeitsicherheitsnachweises. Zwischenbericht. Bundesanstalt für Geowissenschaften
854 und Rohstoffe (BGR), Hannover, Germany, 2013.

855 Ochs M, Mallants D, Wang L. Radionuclide and Metal Sorption on Cement and Concrete. Vol 29.
856 Switzerland: Springer International Publishing, 2016.

857 Pointeau I, Landesman C, Giffaut E, Reiller P. Reproducibility of the uptake of U(VI) onto
858 degraded cement pastes and calcium silicate hydrate phases. Radiochim. Acta 2004; 92:
859 645–650.

860 Ressler T. WinXAS: a program for X-ray absorption spectroscopy data analysis under MS-
861 Windows. J Synchrotron Radiat 1998; 5: 118-122.

862 Richter C, Müller K, Drobot B, Steudtner R, Großmann K, Stockmann M, Brendler V. Macroscopic
863 and spectroscopic characterization of uranium(VI) sorption onto orthoclase and
864 muscovite and the influence of competing Ca^{2+}. Geochim. Cosmochim. Acta 2016; 189:
865 143-157.

866 Rossberg A, Reich T, Bernhard G. Complexation of uranium(VI) with protocatechuic acid -
867 application of iterative transformation factor analysis to EXAFS spectroscopy. Analytical
868 and Bioanalytical Chemistry 2003; 376: 631-638.

869 Rossberg A, Ulrich K-U, Weiss S, Tsushima S, Hiemstra T, Scheinost AC. Identification of Uranyl
870 Surface Complexes on Ferrihydrite: Advanced EXAFS Data Analysis and CD-MUSIC
871 Modeling. Environ. Sci. Technol 2009; 43: 1400-1406.

872 Saleh AS, Lee JY, Jo Y, Yun JI. Uranium(VI) sorption complexes on silica in the presence of calcium
873 and carbonate. J Environ Radioact 2018; 182: 63-69.

874 Schatz T, Kanerva N, Martikainen J, Sane P. Buffer Erosion in Dilute Groundwater. POSIVA 2012-
875 44. Posiva Oy, Eurajoki, Finland, 2013.

876 Schmeide K, Gürtler S, Müller K, Steudtner R, Joseph C, Bok F, Brendler V. Interaction of U(VI)
877 with Äspö diorite: A batch and in situ ATR FT-IR sorption study. Appl Geochem 2014; 49:
878 116-125.

879 Schnurr A. Untersuchungen zur Radionuklidsorption an Tonmineraloberflächen bei hohen
880 Ionenstärken. Fakultät für Chemie und Biowissenschaften. Doctoral Thesis. Karlsruher
881 Institut für Technologie (KIT), Karlsruhe, Germany, 2015.

882 Seher H, Bracke G. Chemische Vorgänge in einem Endlager für hochradioaktive Abfälle in Ton-
883 und Salzgestein. GRS - 301. Gesellschaft für Anlagen- und Reaktorsicherheit (GRS),
884 Cologne, Germany, 2012.

885 Smith KF, Bryan ND, Swinburne AN, Bots P, Shaw S, Natrajan LS, Mosselmans JFW, Livens FR,
886 Morris K. U(VI) behaviour in hyperalkaline calcite systems. Geochim. Cosmochim. Acta
887 2015; 148: 343-359.

888 Steudtner R, Sachs S, Schmeide K, Brendler V, Bernhard G. Ternary uranium(VI) carbonato
889 humate complex studied by cryo-TRLFS. Radiochim. Acta 2011; 99: 687-692.

890 Stumm W. Chemistry of the Solid-Water Interface Processes at the Mineral-Water and Particle-
891 Water Interface in Natural Systems. New York, USA: John Wiley & Sons, Inc., 1992.

892 Sylwester ER, Hudson EA, Allen PG. The structure of uranium (VI) sorption complexes on silica,
893 alumina, and montmorillonite. Geochim. Cosmochim. Acta 2000; 64: 2431-2438.

894 Tits J, Fujita T, Tsukamoto M, Wieland E. Uranium(VI) Uptake by Synthetic Calcium Silicate
895 Hydrates. MRS Proceedings 2008; 1107: 467-474.

896 Tits J, Geipel G, Mace N, Eilzer M, Wieland E. Determination of uranium(VI) sorbed species in
897 calcium silicate hydrate phases: a laser-induced luminescence spectroscopy and batch
898 sorption study. J Colloid Interface Sci 2011; 359: 248-256.

899 Tits J, Walther C, Stumpf T, Mace N, Wieland E. A luminescence line-narrowing spectroscopic
900 study of the uranium(VI) interaction with cementitious materials and titanium dioxide.
901 Dalton Trans 2015; 44: 966-976.

902 Tits J, Wieland E. Actinide Sorption by Cementitious Materials. PSI Bericht Nr. 18-02. Paul
903 Scherrer Institut (PSI), Nuclear Energy and Safety Research Department (NES),
904 Laboratory for Waste Management (LES), Villigen, Switzerland, 2018.

905 Tournassat C, Tinnacher RM, Grangeon S, Davis JA. Modeling uranium(VI) adsorption onto
906 montmorillonite under varying carbonate concentrations: A surface complexation model
907 accounting for the spillover effect on surface potential. Geochim. Cosmochim. Acta 2018;
908 220: 291-308.

909 Troyer LD, Maillot F, Wang Z, Wang Z, Mehta VS, Giammar DE, Catalano JG. Effect of phosphate
910 on U(VI) sorption to montmorillonite: Ternary complexation and precipitation barriers.
911 Geochim. Cosmochim. Acta 2016; 175: 86-99.

912 Tsushima S. On the "yl" bond weakening in uranyl(VI) coordination complexes. Dalton Trans
913 2011; 40: 6732-6737.

914 Tsushima S, Nagasaki S, Tanaka S, Suzuki A. A Raman Spectroscopic Study of Uranyl Species
915 Adsorbed onto Colloidal Particles. J. Phys. Chem. B 1998; 102: 9029–9032.

916 Viallis-Terrisse H, Nonat A, Petit J-C. Zeta-Potential Study of Calcium Silicate Hydrates
917 Interacting with Alkaline Cations. J. Colloid Interface Sci. 2001; 244: 58-65.

Vuorinen U, Lehikoinen J, A. L, Ervanne H. Effects of Salinity and High pH on Crushed Rock and Bentonite – Experimental Work and Modelling. POSIVA 2006-01. Posiva Oy, Olkiluoto, Finland, 2006.

Wang Z, Zachara JM, Boily J-F, Xia Y, Resch TC, Moore DA, Liu C. Determining individual mineral contributions to U(VI) adsorption in a contaminated aquifer sediment: A fluorescence spectroscopy study. Geochim. Cosmochim. Acta 2011; 75: 2965-2979.

Wang Z, Zachara JM, Gassman PL, Liu C, Qafoku O, Yantasee W, Catalano JG. Fluorescence spectroscopy of U(VI)-silicates and U(VI)-contaminated Hanford sediment. Geochim. Cosmochim. Acta 2005; 69: 1391-1403.

Wang Z, Zachara JM, Yantasee W, Gassman PL, Liu C, Joly AG. Cryogenic Laser Induced Fluorescence Characterization of U(VI) in Hanford Vadose Zone Pore Waters. Environ. Sci. Technol 2004; 38: 5591-5597.

Wieland E. Sorption Data Base for the Cementitious Near Field of L/ILW and ILW Repositories for Provisional Safety Analyses for SGT-E2. NAGRA NTB 14-08. National Cooperative for the Disposal of Radioactive Waste (nagra), Wettingen, Switzerland, 2014.

Wolfgramm M, Thorwart K, Rauppach K, Brandes J. Zusammensetzung, Herkunft und Genese geothermaler Tiefengrundwässer im Norddeutschen Becken (NDB) und deren Relevanz für die geothermische Nutzung. Z. Geol. Wiss. 2011; 339: 173-193.

Wolter J-M, Schmeide K, Weiss S, Bok F, Brendler V, Stumpf T. Stability of U(VI) doped calcium silicate hydrate gel in repository-relevant brines studied by leaching experiments and spectroscopy. Chemosphere 2019; 218: 241-251.

Yamamura T, Kitamura A, Fukui A, Nishikawa S, Yamamoto T, Moriyama H. Solubility of U(VI) in highly basic solutions. Radiochim. Acta 1998; 83: 139-146.